ISSN 1063-7788, Physics of Atomic Nuclei, 2021, Vol. 84, No. 4, pp. 483–491. © Pleiades Publishing, Ltd., 2021.

ELEMENTARY PARTICLES AND FIELDS
Experiment

Differential W^+/W^- Cross Section Ratios for W Plus Jet Production in pp Collisions Through (N)NLO in QCD

K. Ocalan[1)*]

Received December 14, 2020; revised December 31, 2020; accepted December 31, 2020

Abstract—This paper presents a phenomenological study of differential W^+/W^- cross section ratios for W-boson production in association with a jet through next-to-leading-order (NLO) and next-to-NLO (NNLO) calculations in perturbative QCD based on the q_T-subtraction approach. The W^+/W^- cross section ratios are calculated for proton–proton collisions at both 8 and 13 TeV energies. The differential distributions for the ratios are presented as functions of important variables that are sensitive to perturbative QCD corrections including the transverse momentum of the W boson, the transverse momentum of the leading jet, and the absolute rapidity of the leading jet. The predicted distributions at (N)NLO accuracy are compared with the 8 TeV data from the ATLAS experiment at the LHC. The differential distributions at 13 TeV are compared at (N)NLO using different parton distribution functions (PDFs) to assess sensitivity of calculations to different PDF models. The presented ratios are found to be under good control by the (N)NLO calculations for most of the phase space regions.

DOI: 10.1134/S1063778821040232

1. INTRODUCTION

W boson production in association with jets (W + jets) is a prominent process and plays a key role at hadron colliders for a thorough understanding of the Standard Model (SM). W bosons decaying leptonically is characterized by a lepton and missing energy that corresponds to either a neutrino or an antineutrino. This process has large production rates and clean experimental signatures in proton–proton (pp) collisions at the CERN Large Hadron Collider (LHC) enabling precision tests for QCD and providing substantial inputs to constrain parton distribution functions (PDFs) in the proton. This process constitutes an important background for rare SM processes including Higgs boson and top quark productions as well as for many new physics searches. In addition to these motivations, W + jets process is used for experimental aspects such as detector calibration and Monte Carlo (MC) tuning studies. The LHC experiments have acquired larger amount of data in more recent years from which several SM results including W + jets have been obtained with reduced experimental uncertainties. In parallel to improvements in experimental accuracy achieved so far for this process from the available LHC data, a considerable work has been carried out on the theory side to provide more precise predictions in line with the experimental results.

In the LHC experiments, differential cross sections for W + jets production $pp \to W^\pm$ + jets $\to l^\pm\nu$ + jets have been measured as functions of several kinematical and angular observables, which are reconstructed from jets and leptonic decay products of the W boson at different center-of-mass energies. These measurements have been provided by the CMS Collaboration using data collected at 7 TeV [1], 8 TeV [2], and 13 TeV [3] and by the ATLAS Collaboration at 7 TeV [4] and 8 TeV [5, 6] as well as by the LHCb Collaboration at 8 TeV [7]. In these complementary measurements, W + jets data have been compared with predictions from various MC event generators and higher-order perturbative QCD calculations comprising either next-to-leading-order (NLO) or next-to-NLO (NNLO) corrections over a large kinematic phase space.

The dominant $W^\pm$ boson production in pp collisions originates from the annihilation of a valence quark with a sea antiquark: $u\bar{d} \to W^+$ and $d\bar{u} \to W^-$. W^+ bosons are therefore produced more often than W^- bosons as a result of the presence of two valence u quarks in the proton causing a production charge asymmetry between W^+ and W^- bosons. $W^\pm$ boson charge asymmetry results based on differential cross section measurements for the inclusive process $pp \to W^\pm \to l^\pm\nu$ have been reported more recently by the CMS [8, 9], ATLAS [10], and

[1)]Faculty of Aviation and Space Sciences, Necmettin Erbakan University, Konya, Turkey.
[*]E-mail: kadir.ocalan@erbakan.edu.tr

LHCb [11, 12] Collaborations at 8 TeV. These results provide input for future PDF determinations particularly providing significant constraints on the valence quark distributions in the proton for certain ranges of the Bjorken scaling variable x. In a similar treatment, W^+/W^- cross section ratios are primarily sensitive to the ratio of u and d valence quark densities that provide valuable information to constrain PDF fits and aid in discriminating among various PDF sets. The measurements of W^+/W^- cross section ratios also enable testing perturbative QCD to greater precision as some of the dominant experimental uncertainties are correlated and cancel in the ratios. The ATLAS Collaboration has performed a differential measurement for W^+/W^- cross section ratios at 8 TeV [6] by using the electron decay channel in association with at least one or two jets $pp \to W^\pm + \text{jets} \to e^\pm\nu + \text{jets}$ as functions of various kinematical variables. This ATLAS paper serves as a main reference for this paper as the (N)NLO ratio predictions at 8 TeV are being compared and validated with its results.

Numerous works have been done to improve theoretical predictions for $W +$ jets process over the years. NLO corrections have been considered in terms of electroweak (EW) corrections [13]. NLO QCD + EW corrections have also been considered in more recent works [14]. Precise theoretical predictions of $W +$ jets process require the inclusion of QCD radiative corrections in the NLO and NNLO calculations. The NLO corrections became already standard for low jet multiplicities and have been automated in NLO + parton shower general-purpose MC event generators [15–17]. The field of NNLO corrections has been growing rapidly for various SM processes including $W +$ jets. The NNLO calculation based on the so-called N-jettiness subtraction method has been available for quite some time for W boson production in association with a single jet ($W +$ jet) [18–20]. In addition, NNLO calculations by means of the antenna subtraction formalism [21] and the jettiness slicing method [22] are also available for $W +$ jet process. Despite the notable progress, only a limited number of approaches has been typically employed to handle the infrared divergences between real and virtual terms in the perturbative QCD expansion of these $W +$ jet NNLO calculations. Different NNLO approaches are needed to validate what has already been done and to go beyond the precision achieved so far down to percent-level, specifically by reducing larger uncertainties in higher regions of kinematic phase space.

This paper presents differential W^+/W^- cross section ratio predictions at NLO and NNLO accuracies for a W boson decaying into an electron(antielectron) and a neutrino(antineutrino) in association with one additional hadronic jet in pp collisions: $pp \to W^\pm + \text{jet} \to e^\pm\nu + \text{jet}$. The cross section ratio calculations are performed in the fiducial phase space of the associated jet and the W boson decay products by using the computational framework MATRIX [23, 24]. The MATRIX framework provides calculations of fully differential cross sections in the form of binned distributions to be compared directly with LHC data. The so-called transverse momentum q_T-subtraction method [25, 26], is employed within the MATRIX framework to control infrared singularities of the final state partons in the NLO and NNLO calculations. The ratios from the differential cross sections are predicted at 8 TeV and compared with the corresponding ATLAS measurement [6] as functions of the important observables including transverse momentum of the W boson p_T^W, the transverse momentum of the most energetic jet (the leading jet) $p_T^{j_1}$, and the absolute rapidity of the leading jet $|y^{j_1}|$. The (N)NLO predictions from different PDF sets for the differential cross section ratios at 13 TeV are presented for the p_T^W, $p_T^{j_1}$, $|y^{j_1}|$, electron(antielectron) transverse momentum p_T^e, and electron(antielectron) absolute pseudorapidity $|\eta^e|$ variables. The p_T^W distribution up to NNLO and the $p_T^{j_1}$, $|y^{j_1}|$, p_T^e, and $|\eta^e|$ distributions up to NLO accuracies are predicted and compared with the ATLAS data at 8 TeV, while the predicted distributions based on several PDF sets are compared at 13 TeV. This paper reports for the first time the W^+/W^- ratios calculated from the predicted differential cross sections at 8 and 13 TeV by using the q_T-subtraction approach along with the (N)NLO calculations for $W +$ jet process. Finally in this paper, the W^+/W^- ratios from the fiducial cross sections are calculated and compared at different perturbative orders up to NNLO.

2. COMPUTATIONAL SETUP

In a fully differential QCD cross section calculation at (N)NLO, evaluation of real and virtual terms is not a trivial task due to the presence of infrared divergences at the intermediate stages of the calculation. The contributions from real and virtual terms cannot be combined in a straightforward manner as divergences affect real and virtual components in different ways. Various approaches have been proposed to overcome this issue [27–31]. The (N)NLO computations with the MATRIX framework in this paper are achieved by a process-independent approach of the q_T-subtraction method for the cancellations of divergences in the cross section calculations. In the q_T-subtraction method, the behavior of the q_T distribution for a system of colorless particles at small

values is known up to NNLO in terms of q_T resummation formalism [32, 33]. The q_T resummation formalism forms a basis for the construction of process-independent infrared subtraction counterterm in the cross section calculation which is applicable to several processes including the $W+$jet production. In the q_T-subtraction method, a residual dependence parameter $r = q_T/m$ is defined by using the invariant mass m of the colorless system. This residual dependence stems from the power-suppressed terms that remain after the subtraction of infrared singularities at finite values and vanish only in the limit $q_T \to 0$. A suitable cut-off value for this residual dependence is employed to render the terms separately finite. In the (N)NLO differential cross section calculations of this paper $r_{\text{cut}} = 0.0015$ (0.15%) is used and below this cut the terms are treated to be identical up to power-suppressed contributions. On the other hand, the fiducial cross sections in this paper are reported for both $r_{\text{cut}} = 0.15\%$ and for the extrapolation in the limit $r_{\text{cut}} \to 0$.

The cross section computation of the $W+$jet production with MATRIX is set up for pp collisions at both 8 and 13 TeV. $W^\pm$ boson production in the electron decay channel ($pp \to W^+ + X \to e^+\nu_e + X$ and $pp \to W^- + X \to e^-\bar{\nu}_e + X$) is used to compare with the corresponding 8 TeV ATLAS measurement [6] presenting the W^+/W^- ratios in the electron decay channel as well. The final state X refers to any other final state including at most one (two) additional parton(s) in the (N)NLO computation. The central values of the renormalization and factorization scales in the computations are fixed to the W boson mass $\mu_R = \mu_F = m(W) = 80.385$ GeV. The scale uncertainties referring to missing higher-order contributions in the computations are estimated by varying independently the μ_R and μ_F by a factor of 0.5 and 2 around the central values. All possible combinations are taken into account in the variations while imposing the constraint $0.5 \le \mu_R/\mu_F \le 2.0$. In the W^+/W^- ratios, this constraint is generalized to an uncorrelated scale variations while restricting to $0.5 \le \mu/\mu' \le 2.0$ between all pairs of scales.

All (spin- and color-correlated) tree-level and one-loop scattering amplitudes are obtained from the OpenLoops tool [34–36] along with the MATRIX (N)NLO computations. The LHAPDF 6.2.0 [37] is utilized for the evaluation of PDFs from data files in the computations. The PDF sets NNPDF30_lo_as_0118, NNPDF30_nlo_as_0118, and NNPDF30_nnlo_as_0118 all with a constant strong coupling $\alpha_s(m(Z)) = 0.118$ are used from the NNPDF Collaboration [38] for the leading-order (LO), NLO, and NNLO cross section calculations, respectively. Main results are obtained from calculations using NNPDF3.0 PDF sets throughout the entire paper. (N)NLO differential distributions at 13 TeV are compared with calculations using CT14 [39], MMHT2014 [40], and ABMP16 [41] (N)NLO PDF sets all with a constant $\alpha_s = 0.118$. The PDF uncertainties for each PDF set are estimated by following the standard prescription of the PDF4LHC working group [37, 42]. The α_s uncertainty is estimated by varying the α_s value by ± 0.001 around the value of 0.118. The total theoretical uncertainties are calculated by summing the scale, PDF, and α_s uncertainties in quadrature. Then, the total uncertainties are symmetrized by taking the larger values from the estimated up and down uncertainties and propagated to the cross section ratio results throughout the entire paper.

3. FIDUCIAL SELECTION

The cross section calculations at both 8 and 13 TeV in this paper are performed by using realistic fiducial cuts that were used in the 8 TeV ATLAS measurement [6]. The (anti)electron is required to have transverse momentum $p_T > 25$ GeV in the absolute pseudorapidity acceptance region of $|\eta| < 2.5$. The anti-k_T jets [43] are used with the distance parameter $\Delta R = 0.4$, where ΔR is defined by using the separation in jet η and in jet azimuthal angle ϕ as $\Delta R = \sqrt{\Delta\eta^2 + \Delta\phi^2}$. The jets are required to have $p_T > 30$ GeV in the absolute rapidity acceptance region of $|y| < 4.4$. Additionally, the jets are selected to refer to all parton-level jets, i.e., gluons and 5 light quarks including a massless bottom quark b such as from the gluon splitting process $g \to b\bar{b}$, which is basically needed to keep jet observables infrared safe. Missing transverse momentum requirement $p_T^{\text{miss}} > 25$ GeV is also applied for all the final state (anti)neutrinos, where p_T^{miss} refers to p_T sum of all (anti)neutrinos. A cut on the W boson transverse mass $m_T(W) > 40$ GeV is also required following the reference ATLAS measurement, where $m_T(W)$ is expressed using the p_T and ϕ variables of (anti)electron and (anti)neutrino as $m_T(W) = \sqrt{2p_T^e p_T^\nu (1 - \cos(\phi^e - \phi^\nu))}$ with p_T^ν and ϕ^ν variables corresponding to the vector of the p_T^{miss}. To this end, the fiducial selection criteria are summarized in Table 1.

4. PHENOMENOLOGICAL RESULTS

The W^+/W^- cross section ratio calculations at both 8 and 13 TeV are performed by using the realistic fiducial selection cuts in line with the 8 TeV ATLAS measurement, as summarized in Table 1.

Table 1. The summary of the fiducial selection cuts used in 8 and 13 TeV cross section ratio calculations

Electron criteria	Jet criteria	p_T^{miss} and $m_T(W)$ criteria
$p_T^e > 25$ GeV	$p_T^j > 30$ GeV	$p_T^{\text{miss}} > 25$ GeV
$\lvert\eta^e\rvert < 2.5$	$\lvert y^j\rvert < 4.4$	$m_T(W) > 40$ GeV

The (N)NLO calculations include total theoretical uncertainties due to μ_R and μ_F scales, PDF choices, and α_s values as described in Section 2. Numerical uncertainties of the calculations are also considered and included together with scale uncertainties for the differential results. Numerical uncertainties amount to ~10–15% of scale uncertainties depending on kinematical variable and region. Total theoretical uncertainties are obtained by summing scale, PDF, and α_s uncertainties in quadrature and are reported together with the central results. The data ratios, that are used in comparisons with 8 TeV ratio predictions, are accompanied with their corresponding experimental uncertainties. The differential ratio distributions are binned by using the binning choices of the 8 TeV ATLAS measurement to facilitate direct comparisons. The differential ratio distributions with their corresponding uncertainties are overlaid in each plot. The ratios of the differential cross section ratios are also included in the lower panels of the plots. The

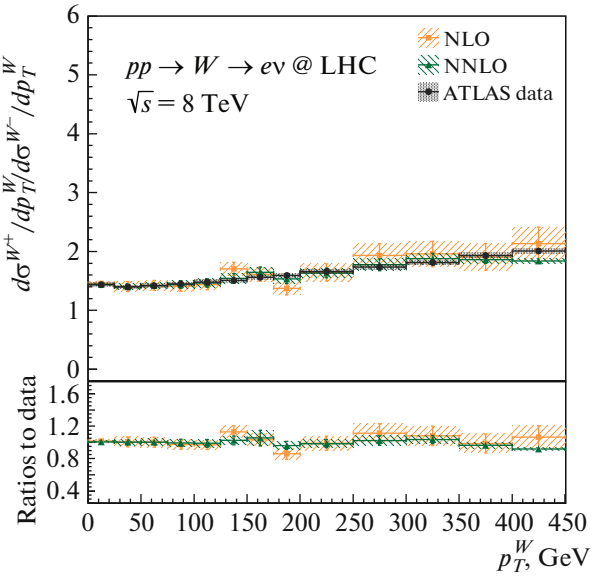

Fig. 1. The differential cross section ratios as a function of p_T^W, $d\sigma^{W^+}/dp_T^W / d\sigma^{W^-}/dp_T^W$, in 0–450 GeV range. The (N)NLO predictions are shown with total theoretical uncertainties and compared with the 8 TeV ATLAS data. The ratios of the predicted W^+/W^- ratios to data are provided in the lower panel.

(N)NLO-to-data ratios are included for the 8 TeV distributions, whereas the ratios of (N)NLO calculations using CT14, MMHT2014, and ABMP16 PDF sets to calculations using NNPDF3.0 PDF set are given for the 13 TeV distributions. Each PDF set is used at appropriate perturbative order, that is LO PDF set is used for LO prediction, NLO PDF set is used for NLO prediction, and NNLO PDF set is used for NNLO prediction. Nonperturbative effects from hadronization and the underlying event are not accounted for by applying nonperturbative corrections in the presented (N)NLO results as these effects cancel out in the W^+/W^- ratios.

First cross section ratios and their comparisons with the 8 TeV ATLAS data are discussed. The differential cross sections are compared for W + jet process as a function of the jet multiplicity N_{jets} up to exclusive one jet in Table 2. The predictions do not include nonperturbative effects and are in agreement with the data in bins of N_{jets}, where the NNLO uncertainties are up to a few-percent level. The differential cross section ratios are compared for the p_T^W up to NNLO in Fig. 1 and the $p_T^{j_1}$ and the $|y^{j_1}|$ up to NLO in Fig. 2. The p_T^W distribution is particularly of importance as its different regions can probe various aspects including resummation and nonpertubative effects in the low-p_T^W region, fixed-order predictions in intermediate- to high-p_T^W regions, and EW Sudakov logarithms at high-p_T^W regions. The (N)NLO predictions are in good agreement with the data for the p_T^W distribution, where NNLO provides better agreement with the data for the entire region. The $p_T^{j_1}$ and $|y^{j_1}|$ distributions are also important as they are sensitive to perturbative QCD corrections. The data distributions are generally better described by NLO throughout the entire $p_T^{j_1}$ and $|y^{j_1}|$ spectra including the higher regions. The uncertainties from the (N)LO predictions become more sizable at high-$p_T^{j_1}$ regions. In all the distributions, (N)NLO provides generally the best descriptions of the data with relatively higher precisions in comparison to (N)LO. The cross section ratios are generally around ~1.4 for lower regions of the distributions and increase towards higher regions consistently in the predictions and data. This observation is important to interpret that W^+ bosons are produced much more than W^- bosons with the increasing values of p_T^W and $p_T^{j_1}$ and also in the forward region of $|y^{j_1}|$.

Next (N)NLO cross section ratios and their comparisons at 13 TeV are discussed. The differential cross section ratios as a function of N_{jets} up to exclusive one jet multiplicity are given in Table 3. The pre-

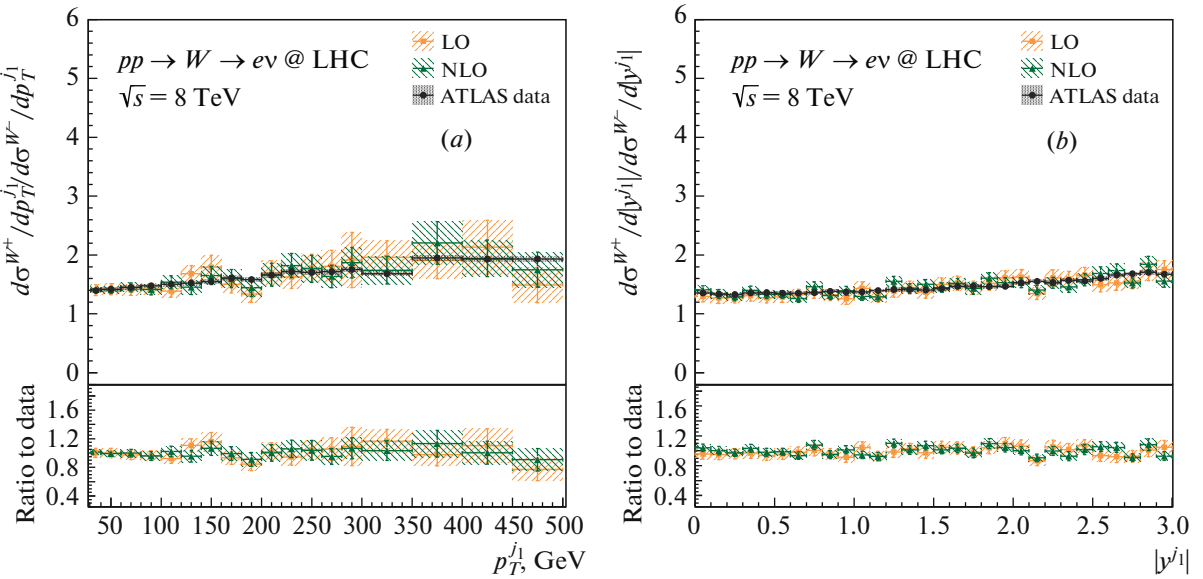

Fig. 2. The differential cross section ratios as a function of $p_T^{j_1}$, $d\sigma^{W^+}/dp_T^{j_1}/d\sigma^{W^-}/dp_T^{j_1}$, in 30–500 GeV range ($a$) and $|y^{j_1}|$, $d\sigma^{W^+}/d|y^{j_1}|/d\sigma^{W^-}/d|y^{j_1}|$ in 0–3.0 range (b). The (N)LO predictions are shown with total theoretical uncertainties and compared with the 8 TeV ATLAS data. The ratios of the predicted W^+/W^- ratios to data are provided in the lower panel.

Table 2. The differential cross sections as a function of N_{jets} for W + jet process, where $W = W^+ + W^-$, calculated exclusively up to one jet; the (N)NLO predictions are accompanied with total theoretical uncertainties and compared with the 8 TeV ATLAS data

N_{jets}	$d\sigma_{\text{NLO}}/dN_{\text{jets}}$	$d\sigma_{\text{NNLO}}/dN_{\text{jets}}$	$d\sigma_{\text{Data}}/dN_{\text{jets}}$
0	4760.81 ± 219.44 pb	4756.00 ± 126.03 pb	4717.00 ± 235.85 pb
1	412.82 ± 51.18 pb	449.60 ± 16.18 pb	436.40 ± 21.80 pb

dicted ratios are consistent between NLO and NNLO calculations with a K-factor analysis of $K_{\text{NNLO}} \simeq 1$, where $K_{\text{NNLO}} = d\sigma_{\text{NNLO}}/d\sigma_{\text{NLO}}$. The NNLO uncertainties are down to ~3.1–3.2% level which is a clear improvement in precision achieved over NLO ones that are in ~5.2–11.4% range. The differential ratios are also investigated as functions of several important variables including p_T^W up to NNLO and $p_T^{j_1}$, $|y^{j_1}|$, p_T^e, and $|\eta^e|$ up to NLO as shown in Figs. 3–5. The (N)NLO predictions using several PDF sets are generally in good agreement with each other within uncertainties for the p_T^W, $p_T^{j_1}$, and $|y^{j_1}|$ distributions. The (N)NLO calculations using CT14 and MMHT2014 PDF sets are more consistent with the calculation using NNPDF3.0 PDF set for the p_T^W and $p_T^{j_1}$ distributions. The predicted uncertainties are more pronounced for higher regions of the p_T^W, $p_T^{j_1}$, and $|y^{j_1}|$ distributions. The ratios in the p_T^W, $p_T^{j_1}$, and $|y^{j_1}|$ distributions increase towards higher regions exhibiting smaller slopes in comparison to the corresponding 8 TeV distributions. The ratio distributions are generally consistent among NLO calculations using several PDF sets for the p_T^e and $|\eta^e|$ spectra. The NLO prediction using ABMP16 PDF set exceptionally exhibits some discrepancies and larger uncertainties as compared to the calculations using NNPDF3.0, CT14, and MMHT2014 PDF sets for the p_T^e distribution. The p_T^e distributions increase in the higher regions as predicted by the NLO calculations. The $|\eta^e|$ distributions are almost flat especially for the lower regions and increase slightly towards the forward regions. In all 13 TeV differential ratio distributions, the level of precision achieved by the calculations using NNPDF3.0, CT14, and MMHT2014 PDF sets are almost comparable. In some regions of the distributions, (N)NLO calculations using ABMP16 PDF set predicted larger uncertainties among the calculations using other PDF sets. Moreover, the ratios of the predicted ratios from calculations using CT14, MMHT2014, and ABMP16 to the predicted ratios from calculations using NNPDF3.0 are around 1 within uncertainties for the bulk of regions of all of

Table 3. The differential cross section ratios as a function of N_{jets}, calculated exclusively up to one jet; the (N)NLO predictions are accompanied with total theoretical uncertainties in percent and compared at 13 TeV

N_{jets}	$d\sigma^{W^+}_{\text{NLO}}/d\sigma^{W^-}_{\text{NLO}}$	$d\sigma^{W^+}_{\text{NNLO}}/d\sigma^{W^-}_{\text{NNLO}}$	K_{NNLO}
0	$1.29 \pm 5.20\%$	$1.31 \pm 3.13\%$	1.02
1	$1.30 \pm 11.37\%$	$1.28 \pm 3.22\%$	0.99

the distributions with only a few exceptions apparent in some regions of the p_T^W, $p_T^{j_1}$, and p_T^e distributions.

Finally fiducial cross section ratios at 8 TeV and 13 TeV are discussed. The ratios are calculated from the cross sections obtained in the fiducial phase space and compared at LO, NLO, and NNLO in Table 4. Two results are reported at (N)NLO based on the r_{cut} value of the q_T-subtraction method as discussed in Section 2. The (N)NLO cross sections are calculated by using a fixed cut-off value of $r_{\text{cut}} = 0.15\%$ and the extrapolation in the limit $r_{\text{cut}} \to 0$. The fiducial cross section ratios are consistent within uncertainties among the perturbative orders. The total uncertainties are significantly reduced at NNLO to 2% level at both 8 TeV and 13 TeV. The best ratio predictions $\sigma^{W^+}_{\text{fiducial}}/\sigma^{W^-}_{\text{fiducial}} = 1.44 \pm 2.1\%$ at 8 TeV and $\sigma^{W^+}_{\text{fiducial}}/\sigma^{W^-}_{\text{fiducial}} = 1.31 \pm 2.3\%$ at 13 TeV are therefore obtained at NNLO either using $r_{\text{cut}} = 0.15\%$ or $r_{\text{cut}} \to 0$ choices. The fiducial cross section ratios are significantly reduced with the increased center-of-mass energy of 13 TeV with respect to 8 TeV. The fiducial ratios are decreased up to $\sim$11.0(9.0)% in going from 8 TeV to 13 TeV according to the (N)NLO calculations. This interpretation is quite consistent with the W^+/W^- fiducial cross section ratios reported separately at 8 TeV [10] and 13 TeV [44] by the ATLAS Collaboration.

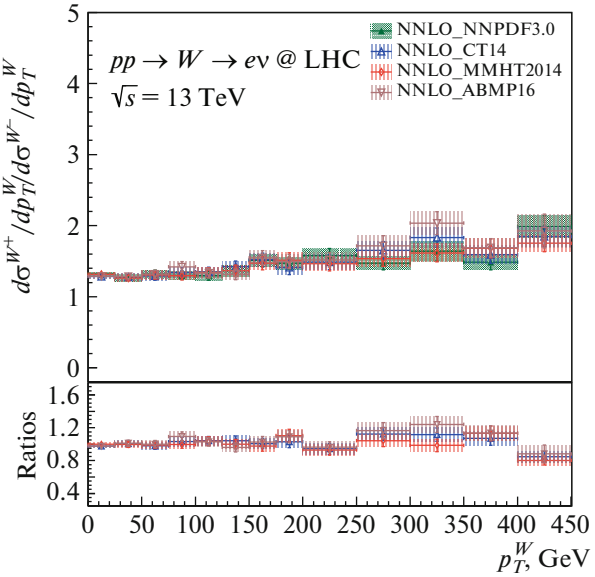

Fig. 3. The differential ratio distributions as a function of p_T^W in 0–450 GeV range. The NNLO predictions are shown with total theoretical uncertainties and compared at 13 TeV. The ratios of the predicted ratios from calculations using CT14, MMHT2014, and ABMP16 PDF sets to the predicted ratios from calculations using NNPDF3.0 PDF set are provided in the lower panel.

Table 4. The W^+/W^- fiducial cross section ratios at both 8 and 13 TeV, calculated at LO, NLO, and NNLO using NNPDF3.0 PDF sets; the (N)NLO cross sections are reported for a fixed cut-off value of $r_{\text{cut}} = 0.15\%$ and for the extrapolation in the limit $r_{\text{cut}} \to 0$; the total theoretical uncertainties are accompanied with the central results in percent

$\sigma^{W^+}_{\text{fiducial}}/\sigma^{W^-}_{\text{fiducial}}$	8 TeV	13 TeV
LO	$1.48 \pm 11.4\%$	$1.33 \pm 14.6\%$
NLO ($r_{\text{cut}} = 0.15\%$)	$1.45 \pm 4.0\%$	$1.30 \pm 4.7\%$
NLO ($r_{\text{cut}} \to 0$)	$1.45 \pm 4.1\%$	$1.28 \pm 4.8\%$
NNLO ($r_{\text{cut}} = 0.15\%$)	$1.44 \pm 2.1\%$	$1.31 \pm 2.3\%$
NNLO ($r_{\text{cut}} \to 0$)	$1.44 \pm 2.2\%$	$1.31 \pm 2.4\%$

5. SUMMARY AND CONCLUSION

A phenomenological study is presented for differential W^+/W^- cross section ratios which offer unique opportunity for tests of perturbative QCD and exploration of partonic content of the proton. The calculations of cross section ratios are performed for the decay channels $W^\pm + \text{jet} \to e^\pm\nu + \text{jet}$ at 8 and 13 TeV LHC pp collisions. The ratios are predicted in the fiducial phase space through NLO and NNLO calculations in perturbative QCD.

The predicted ratio distributions at 8 TeV are compared with the ATLAS measurement [6] differential in p_T^W, $p_T^{j_1}$, and $|y^{j_1}|$ observables. The (N)NLO predictions are generally found to be in good agreement with the ATLAS data, where description of the data for the higher regions of the distributions is noteably improved through the inclusion of (N)NLO corrections. The (N)NLO calculations over (N)LO exhibit higher precision for the bulk of the phase space of the differential ratio distributions. W^+ bosons are produced much more than W^- bosons in the higher kinematic regime in comparison to lower kinematic regime of the distributions. This observation motivates further studies in the field of NNLO calculations, where extreme kinematic regions of $W^\pm$ bosons produced in

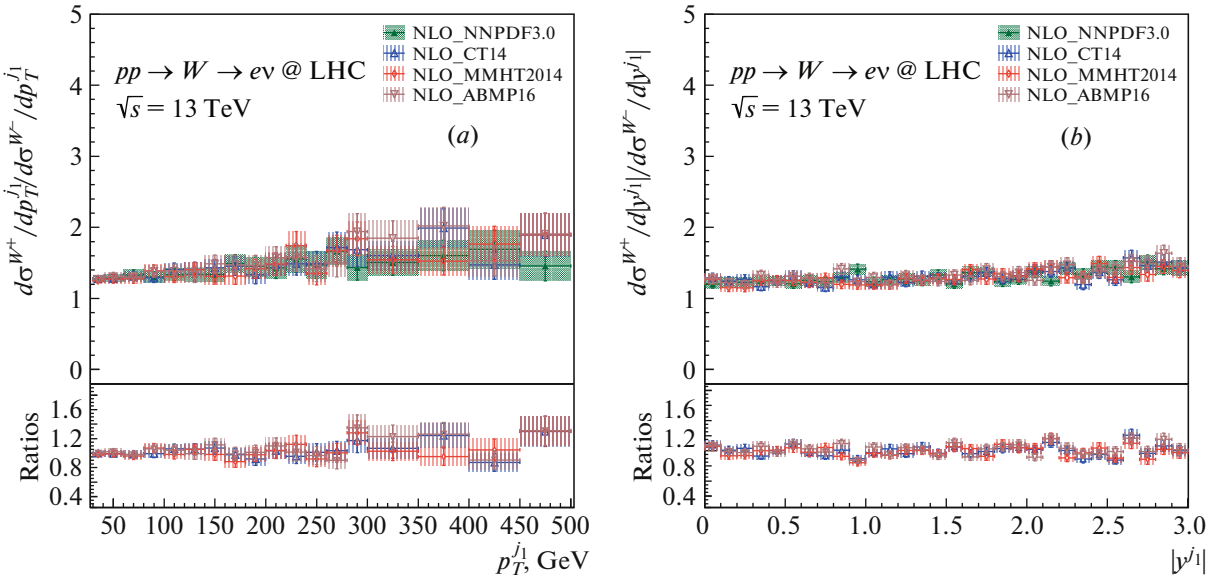

Fig. 4. The differential ratio distributions as a function of $p_T^{j_1}$ in 30–500 GeV range (a) and of $|y^{j_1}|$ in 0–3.0 range (b). The NLO predictions are shown with total theoretical uncertainties and compared at 13 TeV. The ratios of the predicted ratios from calculations using CT14, MMHT2014, and ABMP16 PDF sets to the predicted ratios from calculations using NNPDF3.0 PDF set are provided in the lower panel.

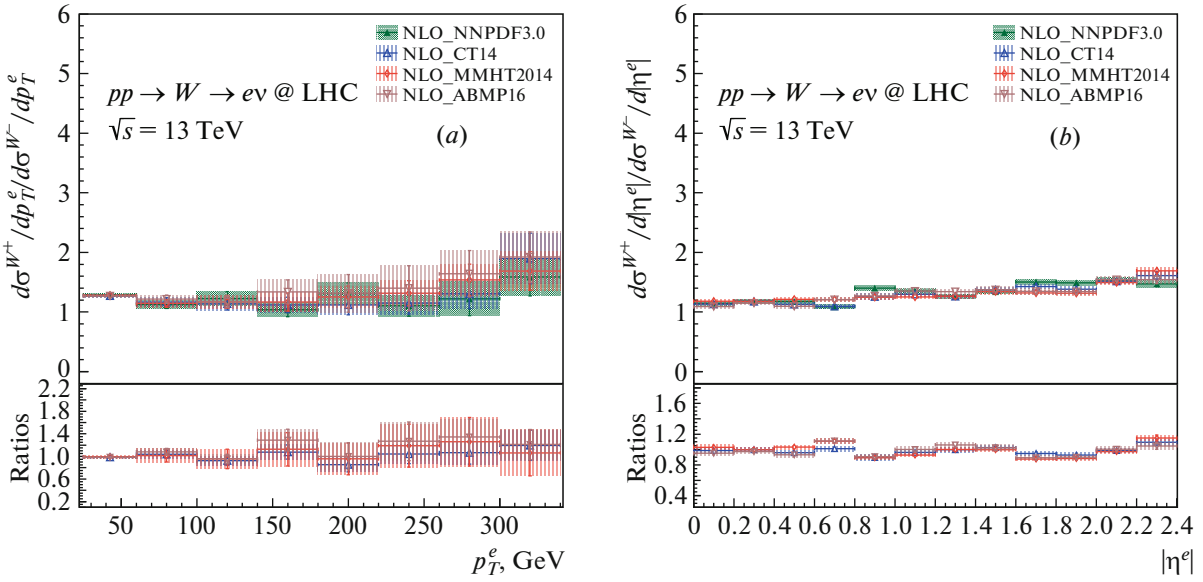

Fig. 5. The differential ratio distributions as a function of p_T^e in 25–340 GeV range (a) and of $|\eta^e|$ in 0–2.4 range (b). The NLO predictions are shown with total theoretical uncertainties and compared at 13 TeV. The ratios of the predicted ratios from calculations using CT14, MMHT2014, and ABMP16 PDF sets to the predicted ratios from calculations using NNPDF3.0 PDF set are provided in the lower panel.

association with a hadronic jet can be benefited to test perturbative QCD much more precisely with a clear focus on reduction of theoretical uncertainties.

The differential ratio distributions at 13 TeV are also provided and compared at (N)NLO using several PDF sets as functions of p_T^W, $p_T^{j_1}$, $|y^{j_1}|$, p_T^e, and $|\eta^e|$ observables. The predicted ratios increase towards higher regions of the distributions exhibiting smaller slopes in comparison to the corresponding predicted distributions at 8 TeV. The ratio distributions shapes are consistently predicted by the calculations using NNPDF3.0, CT14, MMHT2014, and ABMP16 PDF sets for the bulk of regions of the distributions. The (N)NLO calculations using ABMP16 PDF set

exceptionally exhibit some discrepancies and larger uncertainties with respect to the calculations using other PDF sets in some regions of the p_T^W, $p_T^{j_1}$, and p_T^e distributions. The distributions presented in this paper rather suggest using NNPDF3.0, CT14, and MMHT2014 PDF sets for a better prediction of W^+/W^- ratios at (N)NLO accuracy.

The fiducial cross section ratios at 8 and 13 TeV are calculated and compared at LO, NLO, and NNLO accuracies. The NNLO uncertainties are significantly reduced to 2% level at both 8 and 13 TeV results. The best predictions $\sigma^{W^+}_{\text{fiducial}}/\sigma^{W^-}_{\text{fiducial}} = 1.44 \pm 2.1\%$ at 8 TeV and $\sigma^{W^+}_{\text{fiducial}}/\sigma^{W^-}_{\text{fiducial}} = 1.31 \pm 2.3\%$ at 13 TeV are therefore obtained at NNLO accuracy. The fiducial ratios are decreased in going from a lower center-of-mass energy of 8 to 13 TeV at all orders and found to be consistent with the corresponding measurements at 8 TeV [10] and 13 TeV [44] provided by the ATLAS Collaboration.

ACKNOWLEDGMENTS

We would like to thank Marius Wiesemann, one of the authors of the MATRIX, for providing valuable help to set up the computational framework.

REFERENCES

1. CMS Collab. (V. Khachatryan et al.), Phys. Lett. B **741**, 12 (2015).
2. V. Khachatryan et al. (CMS Collab.), Phys. Rev. D **95**, 052002 (2017).
3. A. M. Sirunyan et al. (CMS Collab.), Phys. Rev. D **96**, 072005 (2017).
4. ATLAS Collab. (G. Aad et al.), Eur. Phys. J. C **75**, 82 (2015).
5. ATLAS Collab. (M. Aaboud et al.), Phys. Lett. B **765**, 132 (2017).
6. ATLAS Collab. (M. Aaboud et al.), JHEP **1805**, 077 (2018).
7. LHCb Collab. (R. Aaij et al.), JHEP **1605**, 131 (2016).
8. V. Khachatryan et al. (CMS Collab.), Eur. Phys. J. C **76**, 469 (2016).
9. CMS Collab. (V. Khachatryan et al.), JHEP **1702**, 096 (2017).
10. ATLAS Collab. (G. Aad et al.), Eur. Phys. J. C **79**, 760 (2019).
11. LHCb Collab. (R. Aaij et al.), JHEP **1601**, 155 (2016).
12. LHCb Collab. (R. Aaij et al.), JHEP **1610**, 030 (2016).
13. J. H. Kühn, A. Kulesza, S. Pozzorini, and M. Schulze, Phys. Lett. B **651**, 160 (2007); W. Hollik, T. Kasprzik, and B. A. Kniehl, Nucl. Phys. B **790**, 138 (2008); J. H. Kühn, A. Kulesza, S. Pozzorini, and M. Schulze, Nucl. Phys. B **797**, 27 (2008); A. Denner, S. Dittmaier, T. Kasprzik, and A. Müch, JHEP **0908**, 075 (2009).
14. S. Kallweit, J. M. Lindert, P. Maierhöfer, S. Pozzorini, and M. Schönherr, JHEP **1504**, 012 (2015); S. Kallweit, J. M. Lindert, P. Maierhöfer, S. Pozzorini, and M. Schönherr, JHEP **1604**, 021 (2016).
15. K. Hamilton, P. Nason, and G. Zanderighi, JHEP **1210**, 155 (2012).
16. R. Frederix and S. Frixione, JHEP **1212**, 061 (2012).
17. J. Alwall, R. Frederix, S. Frixione, V. Hirschi, F. Maltoni, O. Mattelaer, H.-S. Shao, T. Stelzer, P. Torrielli, and M. Zaro, JHEP **1407**, 079 (2014).
18. R. Boughezal, C. Focke, X. Liu, and F. Petriello, Phys. Rev. Lett. **115**, 062002 (2015).
19. R. Boughezal, X. Liu, and F. Petriello, Phys. Rev. D **94**, 113009 (2016).
20. J. M. Lindert, S. Pozzorini, R. Boughezal, J. M. Campbell, A. Denner, S. Dittmaier, A. Gehrmann-De Ridder, T. Gehrmann, N. Glover, A. Huss, S. Kallweit, P. Maierhöfer, M. L. Mangano, T. A. Morgan, A. Mück, F. Petriello, et al., Eur. Phys. J. C **77**, 829 (2017).
21. A. Gehrmann-De Ridder, T. Gehrmann, E. W. N. Glover, A. Huss, and D. M. Walker, Phys. Rev. Lett. **120**, 122001 (2018).
22. J. Campbell and T. Neumann, JHEP **1912**, 034 (2019).
23. M. Grazzini, S. Kallweit, and M. Wiesemann, Eur. Phys. J. C **78**, 537 (2018).
24. S. Catani, L. Cieri, G. Ferrera, D. de Florian, and M. Grazzini, Phys. Rev. Lett. **103**, 082001 (2009).
25. S. Catani and M. Grazzini, Phys. Rev. Lett. **98**, 222002 (2007).
26. S. Catani, L. Cieri, D. de Florian, G. Ferrera, and M. Grazzini, Eur. Phys. J. C **72**, 2195 (2012).
27. D. A. Kosower, Phys. Rev. D **57**, 5410 (1998).
28. A. Gehrmann-De Ridder, T. Gehrmann, and E. W. N. Glover, JHEP **0509**, 056 (2005).
29. G. Somogyi, Z. Trócsányi, and V. Del Duca, JHEP **0506**, 024 (2005).
30. R. Boughezal, X. Liu, and F. Petriello, Phys. Rev. D **91**, 094035 (2015).
31. M. Cacciari, F. A. Dreyer, A. Karlberg, G. P. Salam, and G. Zanderighi, Phys. Rev. Lett. **115**, 082002 (2015).
32. J. C. Collins, D. E. Soper, and G. F. Sterman, Nucl. Phys. B **250**, 199 (1985).
33. G. Bozzi, S. Catani, D. de Florian, and M. Grazzini, Nucl. Phys. B **737**, 73 (2006).
34. T. Matsuura, S. C. van der Marck, and W. L. van Neerven, Nucl. Phys. B **319**, 570 (1989).

35. F. Cascioli, P. Maierhöfer, and S. Pozzorini, Phys. Rev. Lett. **108**, 111601 (2012).
36. A. Denner, S. Dittmaier, and L. Hofer, Comput. Phys. Commun. **212**, 220 (2017).
37. A. Buckley, J. Ferrando, S. Lloyd, K. Nordström, B. Page, M. Rüfenacht, M. Schönherr, and G. Watt, Eur. Phys. J. C **75**, 132 (2015).
38. The NNPDF Collab. (R. D. Ball et al.), JHEP **1504**, 040 (2015).
39. S. Dulat, T.-J. Hou, J. Gao, M. Guzzi, J. Huston, P. Nadolsky, J. Pumplin, C. Schmidt, D. Stump, and C.-P. Yuan, Phys. Rev. D **93**, 033006 (2016).
40. L. A. Harland-Lang, A. D. Martin, P. Motylinski, and R. S. Thorne, Eur. Phys. J. C **75**, 204 (2015).
41. S. Alekhin, J. Blümlein, S. Moch, and R. Plačakytė, Phys. Rev. D **96**, 014011 (2017).
42. J. Butterworth, S. Carrazza, A. Cooper-Sarkar, A. De Roeck, J. Feltesse, S. Forte, J. Gao, S. Glazov, J. Huston, Z. Kassabov, R. McNulty, A. Morsch, P. Nadolsky, V. Radescu, J. Rojo, and R. Thorne, J. Phys. G **43**, 023001 (2016).
43. M. Cacciari, G. P. Salam, and G. Soyez, JHEP **0804**, 063 (2008).
44. ATLAS Collab. (G. Aad et al.), Phys. Lett. B **759**, 601 (2016).